*DISTRIBUTION STATEMENT A. Approved for public release; distribution is unlimited.*

# Analysis of Coherent Microwave Data Collected on the Ocean over Two Decades

William J. Plant
Applied Physics Laboratory
University of Washington
1013 NE 40th St
Seattle, WA 98105-6698
phone: 206-543-7836 fax: 206-543-6785 plant@apl.washington.edu

Grant # N00014-10-10318
http://airs.apl.washington.edu/personnel/personnel.html

## LONG-TERM GOALS

The long-term goal of this project is to fully utilize microwave backscattering data sets that have been collected on the ocean over the last two decades. The prime objective is to better understand the formation of breaking waves on the ocean and their effect on microwave backscatter.

## SCIENTIFIC OBJECTIVES

The scientific objectives of this research are to investigate experimentally wave shadowing and modulation in low-grazing-angle backscatter from the ocean.

## APPROACH

Our approach is to reanalyze data sets taken with Doppler radars over the last two decades in an attempt to extract additional information on microwave backscatter from the ocean. These data sets have been taken on a variety of platforms from airplanes and towers to blimps and ships using a variety of coherent microwave radars. In the particular work that has been carried out in the past year, we have looked for evidence of shadowing of microwave backscatter by ocean waves and have applied bound/breaking wave theory to observed phase differences between modulated received power and scatterer velocities.

## WORK COMPLETED

Several data sets collected over the past two decades were examined to see if they supported a geometric shadowing picture of low-grazing-angle backscatter from the ocean. We may consider effects of the possible types of rough-surface shadowing on the modulation of backscattered power by ocean waves as shown in Figure 1. Incoming rays are indicated by slanting lines from the left. Figures 1a and c show geometric shadowing at low and high incident power levels. Increasing the incident power can only increase the return in the illuminated areas. By the very definition of geometric shadowing, the change in power level cannot affect the regions that are not illuminated so the probability of observing signals at the noise level cannot change. Also note that geometric shadowing

is a ray theory so the polarization of the incident radiation is irrelevant. By contrast, Figures 1b and d show cases of partial shadowing at low and high incident power levels. In this case, backscatter can come from the areas that are geometrically shadowed but may be reduced either because the incident field is reduced or because scatterers in this region are weaker than in the illuminated areas due to their modulation by waves. Both of these processes may be polarization dependent. If the incident power level is low, the radar may still observe signals at the noise level in areas behind a crest as shown in Figure 1b. In practice, the difference between the modulations of received power diagrammed in Figures 1a and b may be difficult to distinguish. However, for partial shadowing, an increase in the incident power level may raise the backscatter from behind the crests above the noise level as shown in Figure 1d. Thus either changing the incident power level or noting polarization differences may allow differentiation between geometric and partial shadowing.

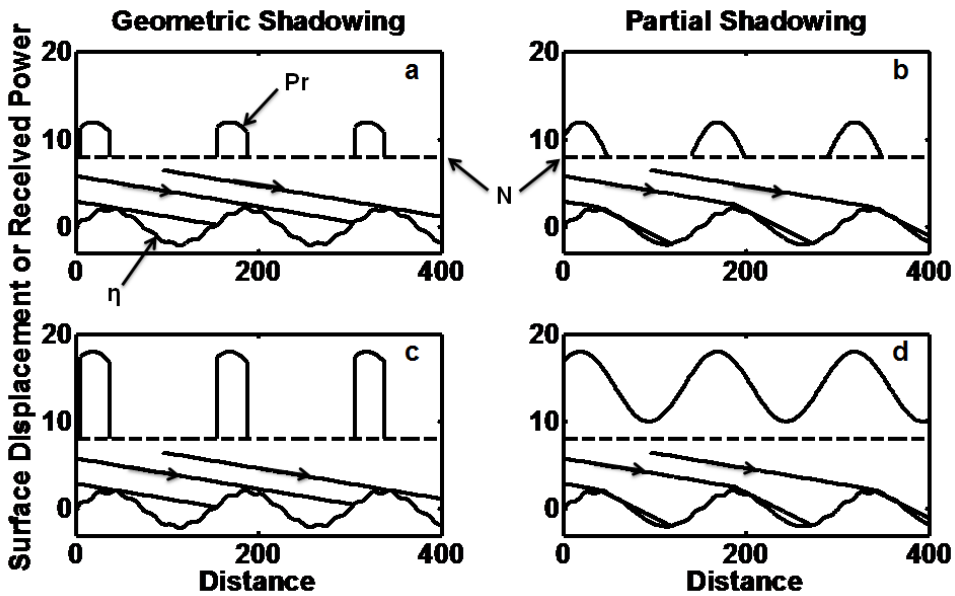


***Figure 1. Diagrams of geometric and partial shadowing at low and high incident power levels.***

$P_r$ is received power, N is the radar noise level indicated by the dashed line, and η is the sea surface. a) geometric shadowing, low incident power; b) partial shadowing, low incident power; c) geometric shadowing, high incident power; d) partial shadowing, high incident power.

For all of the data collected with our radars, we computed the signal-to-noise ratio, SNR:

$$\mathrm{SNR} = \frac{P_r' - N}{N} = \frac{P_r}{N}$$

where $P_r'$ is the received power from the sea surface plus noise. We then determined the fraction of the data from various runs that had SNR<1. We will call this fraction the concealed fraction since the signal, if any, is smaller than the system noise and therefore concealed from detection. Each sample of received power was averaged only over the time that the radars took to collect them, either 262 msec

or 41 msec. Each data set contained in excess of 300 data points at each range bin, each of which yielded a value of SNR. The number of SNR values less than one was then determined and divided by the total number of samples for that range bin for that run.

Average SNR values in dB divided by 100 and the concealed fractions at various ranges for HH polarized data collected on an airship in 1995 are shown in Figure 2. The antenna height was 240 m so the grazing angles for the ranges shown are from 25.2$^o$ to 71.6$^o$. In this range of grazing angles, shadowing is not expected and the concealed fraction becomes non-zero only where the incident power is low. This shows that, as expected, weak scatterers can produce very low backscatter even in the absence of shadowing if the incident power level is low.

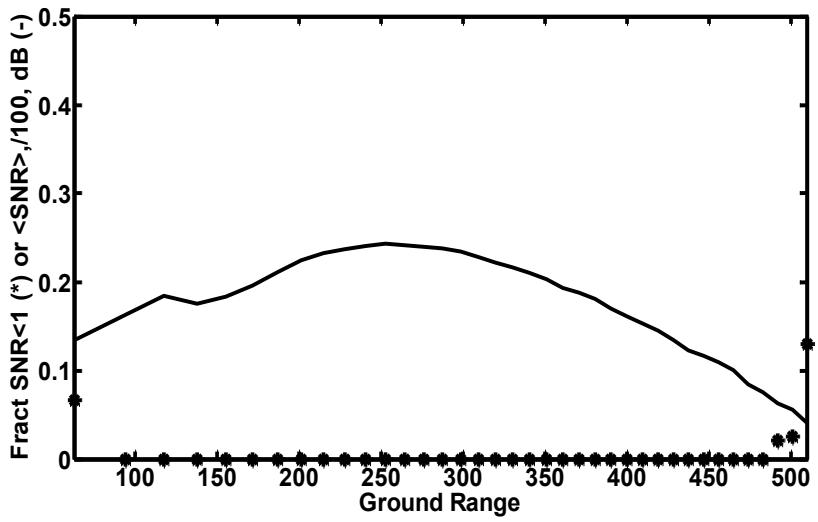


***Figure 2. Data collected on the airship in 1995 with HH polarization for grazing angles between 25.2$^o$ and 71.6$^o$. The solid curve is the average signal-to-noise ratio, SNR, in dB divided by 100 and the asterisks show the fraction of SNR values having SNR<1, the concealed fraction. Wind 12.6 m/s from 173$^o$T, antenna boresite 55$^o$ looking toward 180$^o$T. Range resolution in 7.5 m.***

Figure 3 shows VV polarized data taken on the R/V Thompson in 2008 at very low grazing angles. Now the concealed fraction is significant even where the incident power is high. This could indicate that some geometric shadowing is taking place. However, the concealed fraction exhibits much different behavior than predicted by Milder (2004) whose result is shown as the dashed line in Figure 3. This was computed as the fraction shadowed

$$f_s = 1 - f$$

where f is Milder's fraction illuminated, which he gives in his Eq.3.7 as

$$f(\alpha) = \sqrt{2\pi}(\alpha/\sigma)$$

where α is the tangent of the grazing angle and σ is the rms slope of the rough surface. Milder

says that this result is valid when $\alpha \ll \sigma$. We show values when $\alpha/\sigma < 1/\sqrt{2\pi}$. For σ we have used the wind-speed dependent results of Cox and Munk (1954) for a slick-covered surface, which makes σ as small as possible and therefore $f_s$ as small as possible. We see that even using this small rms slope, the predicted fraction shadowed is generally larger than observed concealed fraction except at grazing angles in the near range where the theory says that geometrical shadowing should not occur. Furthermore, in the data, the concealed fraction decreases with increasing wind speed while the theory predicts the opposite. If the theory is correct, and other theories of geometric shadowing are very similar, then again geometrical shadowing does not appear to explain the observations.

In the data discussed so far, the decrease in incident power for any particular set of environmental and radar parameters was always correlated with a decrease in grazing angle. Thus it could be argued that the increase in concealed fraction at far ranges could be due to the decreasing grazing angle, and subsequent increasing shadowing, rather than to the decreasing incident power. To investigate this possibility, we examined data taken on the Ocean Researcher 1 in the South China Sea in 2007 at a wind speed of 11.7 m/s and very low grazing angles. The pitching of the ship varied the boresite of the antennas. Because pencil-beam antennas were used, this pitching had a large effect on the signal-to-noise ratio. In order to determine the boresite during data collection, we smoothed the received power in range and found the range at which it maximized. Modeling the backscatter using the radar equation and estimates of the NRCS allowed us to determine the antenna boresite from the range at maximum received power. Figure 4 shows the result of binning the backscatter into two boresite ranges that were $1^o$ apart. In the boresite range $0^o$ to $0.5^o$ (Figure 4a), the average SNR was higher and the concealed fraction was lower than in the boresite range $1^o$ to $1.5^o$ (Figure 4b) for every range above 1000 m. Yet the grazing angle at any particular range was the same for both boresites. This shows that the increase in concealed fraction is due to the decreased incident power for larger boresites and not due to a change in grazing angle. This is true both for HH and VV polarization, again indicating partial shadowing, not geometric shadowing.

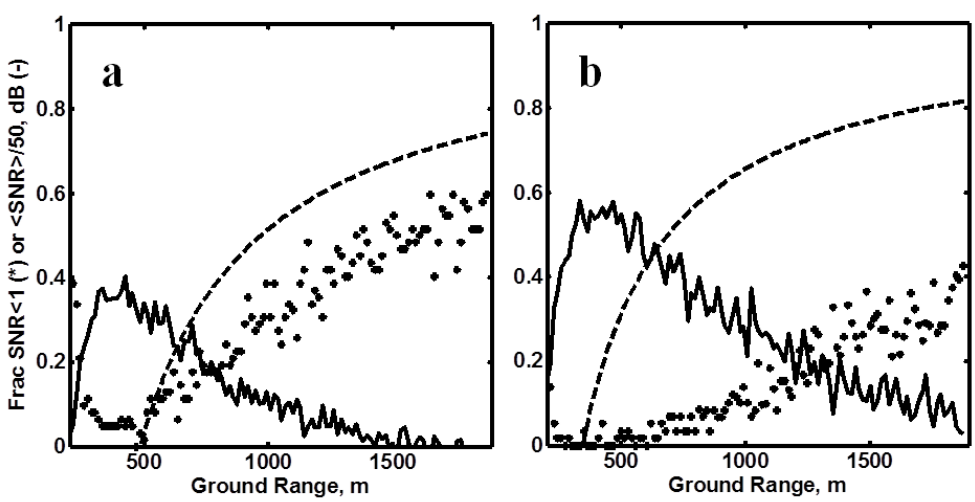


***Figure 3. Average SNR in dB divided by 50 (solid curve) and concealed fractions (asterisks) as function of range for data taken on the R/V Thompson at VV polarization. The dashed curves are the predictions of Milder's geometrical shadowing theory discussed in the text. a) Wind 7.3 m/s from $9^o$T, antenna boresite $1^o$ to $2^o$ looking toward $7.5^o$T. b) Wind 16.9 m/s from $341^o$T, antenna boresite $1^o$ to $2^o$ looking toward $342.5^o$T. Range resolution in 7.5 m***

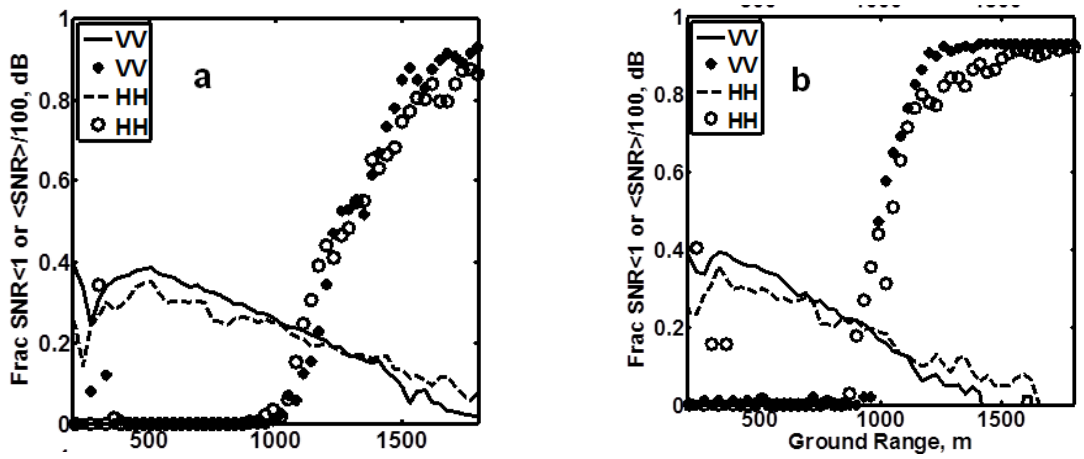


***Figure 4. Average SNR in dB divided by 100 and concealed fractions for two different boresite angles (top and bottom) for data taken on the OR1 in 2007. Wind: 11.7 m/s from 25$^o$T. a) Boresite = 0.0$^o$ to 0.5$^o$ looking toward 51$^o$T. b) Boresite = 1.0$^o$ to 1.5$^o$ looking toward 51$^o$T. Range resolution is 30 m.***

Figure 5 shows the magnitude and phase of the coherence functions for HH and VV polarization looking upwind and downwind for data taken in the South China Sea. This data set was collected with a 30 m range resolution so only modulation by waves longer than 60 m can be observed in the coherence function. We consider up/down wave to be up/down wind. In the figure, positive phases indicate that maxima of received power modulations occur at shorter ranges than maxima of scatterer velocity modulations. The figure shows a clear dependence of the phase between received power and scatterer velocity on both look direction and polarization.

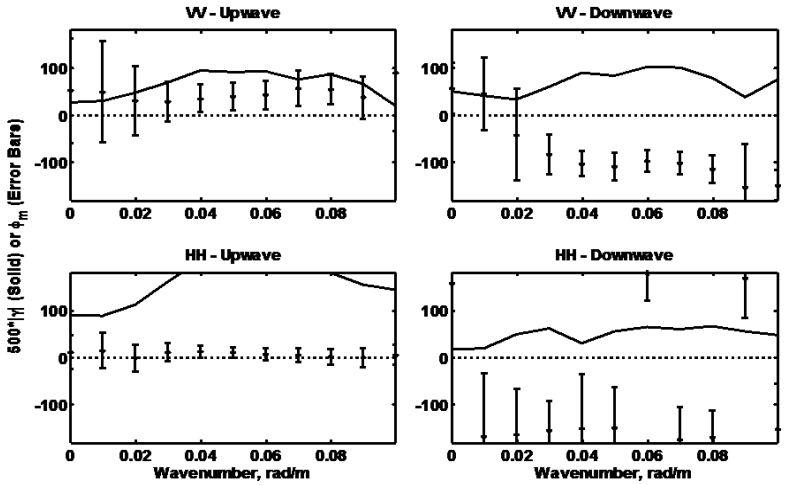


***Figure 5. Magnitude and phase of the coherence function between wave-induced variations in received power and scatterer velocity. Magnitudes are solid lines and phases are asterisks with 95% intervals shown. Upwave and downwave measurements were made within three hours of each other. The wind speed was 10.6 m/s from 45 $^o$T and the antenna looked toward 45 $^o$T during the upwave measurements. The wind had not changed but the antenna looked toward 225 $^o$T during the downwave measurements.***

We can model the expected result of wave modulation on a bound wave/free wave picture similar to that invoked earlier in both open ocean and wave tank studies (Plant, 1997; Plant et al., 1999a, 1999b, 2004). The idea is that long waves on the ocean both modulate free, wind-generated capillaries, as the standard composite surface model postulates, and cause intermediate scale waves to break, producing bound or breaking waves. The resultant backscatter is the sum of these processes. Both processes vary with position on the long wave and we simplify the problem by considering these variations only to first order in long wave slope. Then for a sinusoidal long ocean wave,

$$\eta = A \exp\{-i(\mathbf{k}\cdot\mathbf{R}-\omega t)\}$$

we write the (detrended) wave-modulated power and velocities as

$$P_r = \langle P_r \rangle \{F_f [m_h + m_t] + F_b m_b\} k\eta$$
$$V_s = \{F_f + F_b m_v\}\ \boldsymbol{\kappa}\cdot\mathbf{C} k\eta$$

where **C** is the long wave phase speed, $\boldsymbol{\kappa}$ is a unit vector in the antenna-look direction, < > indicates an average over the time series, $F_f$ is the fraction of backscatter due to free waves, $F_b$ is the fraction of backscatter due to bound/breaking waves, and $k = 2\pi/L$ where L is long-wave length. Note that $F_f + F_b = 1$. The different types of modulation transfer functions are $m_h$, the hydrodynamic MTF of the free waves; $m_t$, the tilt MTF of the free waves; $m_b$, the bound/breaking wave MTF. The free waves are advected by the long wave orbital velocity, which is written $\mathbf{C}k\eta$. The transfer function $m_v$ accounts for the fact that the amplitude and phase of the bound wave velocity variation is not the same as the long wave orbital velocity. The amplitude of the bound wave velocity is the phase speed of the parent wave producing the bound waves. Phases of the modulations are with respect to the long wave crest and are positive in the direction of wave travel.

The hydrodynamic MTF includes both the modulation of the freely propagating short wave amplitudes and range changes caused by the long wave amplitudes; both are in phase with the long wave. The orbital velocity is also in phase with the long wave. The tilt mtf is always $90^o$ out of phase with the long wave and occurs on the side of the crest toward which the antenna is looking. Finally, Plant (1997) found that the maximum of $m_b$ occurred approximately$130^o$ in front of the long wave crest. We therefore model these MTFs as follows:

$$m_h = 2+3/(hk)$$
$$m_t = 15 \exp[+i\pi/2], \qquad \text{upwave}$$
$$m_t = 15 \exp[-i\pi/2], \qquad \text{downwave}$$
$$m_b = 2 \exp[i2\pi(130/180)]$$
$$\mathbf{C} = \sqrt{g/k}$$
$$m_v = (1.5/C) \exp[i2\pi(130/180)]$$

where h is the height of the antenna.

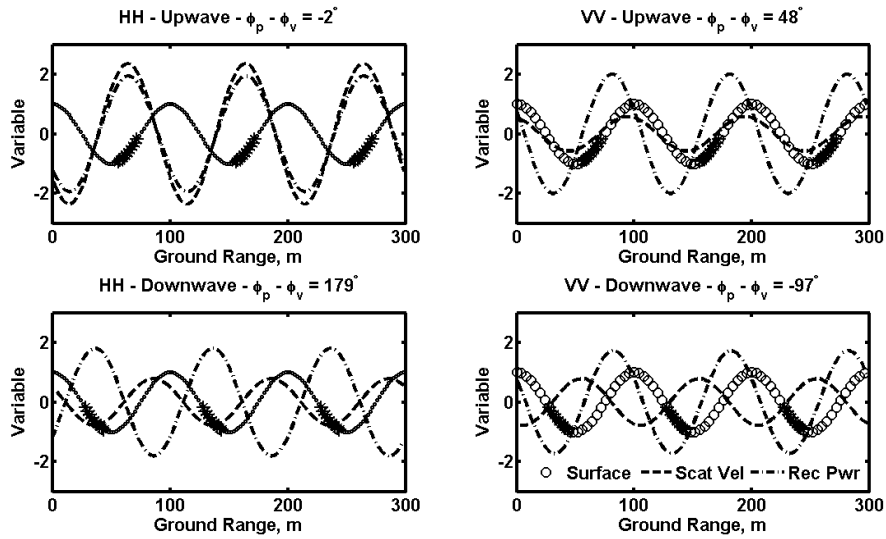


***Figure 6. Simulated modulations of received power and scatterer velocity by a sinusoidal long wave of 1 m amplitude and 100 m wavelength. The circles and asterisks are located on the surface, circles indicating wind waves and asterisks indicating breaking waves. The relative size of the circles and asterisks indicates their importance in HH and VV backscatter. The dashed curve shows the modulated velocity, and the dash-dotted curve shows the modulated power. Waves in the upper panels move to the left, toward the radar, while those in the lower panels move to the right, away from it. The phase differences between power and velocity, $\varphi_p$ - $\varphi_v$, shown in the figure agree with the measurements shown in Figure 10 to within about $10^o$.***

We may now determine the behavior of the phase of the correlation function for different polarizations and look directions. We take $F_f = 0.9$ looking upwind and $F_f = 1$ looking downwind. For HH polarization the bound/breaking waves are dominant but a small feature at free wave frequencies can be seen. Therefore, we take $F_f = 0.15$ looking upwind and $F_f = 0.3$ looking downwind. We illustrate the modulation process using a long wave with A = 1 m and L = 100 m.

Figure 6 shows the result of this simple, linear simulation. Even though the model is surely too simple, especially for the bound/breaking waves, the phase differences between received power and scatterer velocity modulations are close to those shown in Figure 10 in all cases. One can see that power and velocities maximize in most cases in regions where geometric shadowing would predict no backscatter (see Figure 1). For VV polarization, the bound/breaking waves make only a minor difference, the shift from $\pm 90^o$ phases upwind and downwind being mostly due to the hydrodynamic modulation of the free waves. For HH polarization, on the other hand, bound/breaking waves are crucial.

## REFERENCES

Milder, D.M., Surface shadowing at small grazing angles, Waves Random Media, 13, 89-94, 2003.

Plant, W.J.. A model for microwave Doppler sea return at high incidence angles:
Bragg scattering from bound, tilted waves, J. Geophys. Res, 102(C9), 21131-21146, 1997.

Plant, W.J., W.C. Keller, V. Hesany, T. Hara, E. Bock, and M. Donelan. Bound waves and Bragg scattering in a wind wavetank, J. Geophys. Res., 104(C2), 3243-3263, 1999a.

Plant, W.J., "Crumpling" wave effects in backscatter from the air-sea interface, in The Wind-Driven Air-Sea Interface, edited by M.L. Banner, Univ. New South Wales, 409-416, 1999b.

Plant, W.J., P.H. Dahl, J.P. Giovanangeli, H. Branger, Bound and free surface waves in a large wind-wave tank, J. Geophys. Res., 109, C10002, doi:10.1029/2004JC002342, 2004.

## IMPACT/APPLICATION

It is common to think of low-grazing-angle backscatter from the ocean in terms of geometric shadowing. This work shows that on the open ocean this is a very bad model. In fact, our work indicates that on the open ocean no evidence exists to indicate that any reduction at all in the incident fields takes place in geometrically shadowed regions at either VV or HH polarization. Therefore models of low-grazing-angle backscatter will have to focus on more realistic causes in regions of very low backscatter, such as very low scatterer intensities. They cannot simply be brushed aside as "shadowed regions'.

## TRANSITIONS

The results of this project have not yet been transitioned for operational use.

## RELATED PROJECTS

The work carried out in this project to date is closely related to projects aimed at measuring waves around ships because it addresses the causes of wave modulation at both HH and VV polarization. The relevant projects are ONR's Ship Guidance MURI and Hi Res DRI and the ongoing, more applied projects in the Environment and Ship Motion Forecasting program.